Research Square

Preprints are preliminary reports that have not undergone peer review.
They should not be considered conclusive, used to inform clinical practice,
or referenced by the media as validated information.

Spatiotemporal Defect Dynamics and Microstructural Hierarchy under Extreme Shear

Arun Devaraj

arun.devaraj@pnnl.gov

Pacific Northwest National Laboratory https://orcid.org/0000-0003-1314-6212

Tingkun Liu

Pacific Northwest National Laboratory

Changyong Park

ANL https://orcid.org/0000-0002-3363-5788

Stanislav Sinogeikin

Carnegie Institution of Washington

Matthew Olszta

Pacific Northwest National Laboratory (PNNL)

Bharat Gwalani

North Carolina State University https://orcid.org/0000-0002-3021-6676

Lei Li

Pacific Northwest National Laboratory https://orcid.org/0000-0002-2688-1243

Nanjun Chen

University of Michigan

Qin Pang

Pacific Northwest National Laboratory

Wenkai Fu

Pacific Northwest National Laboratory

Semanti Mukhopadhyay

Pacific Northwest National Laboratory

Suveen Mathaudhu

Colorado School of Mines

Yulan Li

Pacific Northwest National Laboratory

Ayoub Soulami

Pacific Northwest National Laboratory

Shenyang Hu

Pacific Northwest National Laboratory

Peter Sushko

Pacific Northwest National Laboratory https://orcid.org/0000-0001-7338-4146

Cynthia Powell

Pacific Northwest National Laboratory

Physical Sciences - Article

Keywords:

Posted Date: March 30th, 2026

DOI: https://doi.org/10.21203/rs.3.rs-8768356/v1

License: This work is licensed under a Creative Commons Attribution 4.0 International License.
Read Full License

Additional Declarations: There is **NO** Competing Interest.

Spatiotemporal Defect Dynamics and Microstructural Hierarchy under Extreme Shear

Arun Devaraj[1, 2*], Tingkun Liu[1], Changyong Park[3], Stanislav Sinogeikin[4], Matthew Olszta[5], Bharat Gwalani[6], Lei Li[5], Nanjun Chen[1], Qin Pang[1], Wenkai Fu[1], Semanti Mukhopadhyay[1], Suveen Mathaudhu[2, 5], Yulan Li[1], Ayoub Soulami[5], Shenyang Hu[5], Peter V. Sushko[1], Cynthia Powell[5]

[1]Physical and Computational Science Directorate, Pacific Northwest National Laboratory

[2]Metallurgical Engineering, Colorado School of Mines

[3]High Pressure Collaborative Access Team, X-ray Science Division, Argonne National Laboratory

[4]DAC Tools LLC

[5]Energy and Environment Directorate, Pacific Northwest National Laboratory

[6]Department of Material Science and Engineering, North Carolina State University

*Corresponding author: arun.devaraj@pnnl.gov

Summary:

Understanding the dynamic microstructural evolution of materials under extreme shear deformation is crucial for advancing severe plastic deformation processing, tribology, and geology[1-8]. Despite decades of research leveraging ex situ experimental analysis and simulations, significant knowledge gaps persist regarding critical processes like grain boundary sliding and changes in dislocation density and vacancy concentration under high-speed shear[3,9,10]. This is largely due to the challenges of capturing real-time microstructural changes during rapid shear deformation[11]. To address this, here we developed a high-speed rotational diamond anvil cell for in situ synchrotron X-Ray diffraction studies. Integrating these in situ insights with multimodal ex situ characterization and multiscale computational simulations, we unravel the mechanisms of defect evolution, hierarchical microstructural refinement, and deformation-induced intermixing in a model Cu–Ni powder mixture. Capturing these rapid, previously hidden, phenomena pave the way for fresh insights into material behavior under extreme conditions, revealing fundamental mechanisms of deformation that were hitherto inaccessible.

Main:

Extreme shear-driven microstructural changes underpin advances in severe plastic deformation routes, tribological interfaces, and geological processes[1-5,8]. This knowledge is key to comprehending and controlling the microstructural changes occurring during severe plastic deformation-based material processing methods such as friction stir processing, friction extrusion, equal channel angular pressing and high-pressure torsion[5-7]. In tribology, this understanding aids in creating materials and surfaces with enhanced friction control, wear resistance, and durability, leading to improved performance and energy efficiency of mechanical systems[4,8]. Additionally, it

sheds light on critical geological processes that results from extreme shear deformation of minerals, including fault dynamics, earthquake mechanisms, and metamorphic rock formation[1,10,12].

To date, researchers have primarily relied on observations of material microstructures before and after extreme shear deformation, combined with computational simulations, to infer the dynamic evolution of these microstructures.[3,9]. Although these approaches have advanced our understanding, important questions remain. For example, we still need to determine (i) how vacancy concentrations evolve during high-speed shear deformation, whether these concentrations decrease once the shear stops, and how such changes influence atomic diffusion in real time; (ii) how to accurately quantify dislocation density both during and immediately after deformation; (iii) what role grain boundary sliding and migration play in promoting compositional intermixing across interfaces; and (iv) how microstructural refinement evolves during extreme shear.

The range of length and time scales involved in these processes has made it difficult to develop predictive models that integrate hierarchical microstructural information. These challenges largely stem from the experimental difficulty of directly observing material changes at the atomic or micron scale during high-speed shear. Consequently, it is critical to develop and refine in situ experimental techniques for studying microstructural evolution under these extreme conditions. Addressing the remaining gaps will also require integrating in situ approaches with ex situ multi-scale microstructural characterization and improved multiscale simulations to achieve a deeper mechanistic understanding. Ultimately, advances in these areas may lead to novel material processing methods that exploit extreme high-speed shear deformation to engineer unique microstructures with superior mechanical and functional properties.

One promising approach for the in situ analysis of microstructural evolution during shear deformation using synchrotron X-ray diffraction is the use of rotational diamond anvil cells (RDACs)[11]. These devices allow one diamond anvil to rotate perpendicular to the compression axis while the other remains fixed, thereby generating significant shear stress and strain on the sample placed between the diamond anvils[13]. Previous studies using RDACs at synchrotron beamlines, albeit at slow rotation speeds have shown that shear deformation can markedly reduce transformation pressure, change reversible phase transformations into irreversible ones, produce phases not achievable under hydrostatic conditions, and induce strain-controlled kinetics[14-19]. However, existing RDAC experiments have been limited to quasistatic shear conditions. Consequently, they are ill-suited for investigating the dynamic microstructural evolution during high-speed shear deformation, leaving a technological gap in our ability to capture these rapid changes with high temporal and spatial resolution.

To address these persistent knowledge and technological gaps, we developed a novel high-speed rotational diamond anvil cell (HSRDAC). We implemented the HSRDAC at a synchrotron X-ray beamline to enable in situ investigations of microstructural hierarchy evolution in materials. For our study, we selected a Cu-Ni powder mixture, a well-established miscible alloy system, as a candidate to explore how deformation accelerates mixing and to unravel the elementary mechanisms driving this process[20].

Results and Discussion

Figure 1 illustrates the key results from our experiments using a novel high-speed rotational diamond anvil cell (HSRDAC). Figure 1A presents a schematic of the experiment, with Figure 1B highlighting a photograph of the HSRDAC installed at the synchrotron beamline. A 50-50 Cu-Ni wt.% powder mixture was loaded between two 500 μm culet diamonds, confined within a 125 μm radius sample cavity by a pre-indented, laser-drilled stainless-steel gasket. Static X-ray diffraction imaging (XDI) of the compacted Cu–Ni powder before shear (left image in Figure 1C) reveals clearly defined Cu and Ni domains. XDI (right Figure 1C) after applying shear deformation (10 RPM for 1 minute) shows the emergence of a circular vortex that indicated shear-induced mixing of the Cu and Ni powders.

To capture the dynamic microstructural evolution during shear, we collected in situ X-ray diffraction (XRD) spectra at a position ¼ diameter of the sample (60 μm from the center of the sample) during a 5-minute shear experiment at 10 RPM, with one diffraction pattern collected every 10 seconds (Figure 1D) with 0.4 second exposure time. Analysis of these dynamic spectra allowed us to derive evolution of Cu and Ni lattice strain (Figure 1E) Throughout the test, Cu consistently exhibited higher compressive strain than Ni.

A quantitative comparison of the full width at half maximum (FWHM) for these peaks, tracked continuously during shear (0 to 5 minutes) and immediately thereafter (at 1, 2, and 5 minutes; Figure 1F), confirmed that the increased peak broadening during shear is attributable to both grain refinement and an elevated defect density. Additionally, an overlay of the Cu (200) and Ni (200) diffraction peaks, acquired immediately before (dynamic) and after (static) shear illustrated that the peak widths broaden during shear and once shear is halted, they rapidly narrow (Figure 1G). The prompt recovery of the peak widths on halting shear is consistent with earlier observations by Kilmametov et al., who linked such behavior to a transient increase in vacancy concentrations under shear conditions similar to that of an alloy near its melting point.[21]

Finally, using the in situ XRD data, we quantified the dislocation density dynamically during shear and observed a clear reduction immediately after the shear stopped (Figure 1H). These results collectively demonstrate the capability of the HSRDAC to capture rapid microstructural changes with high temporal and spatial resolution, thereby bridging the technological gap identified in earlier studies.

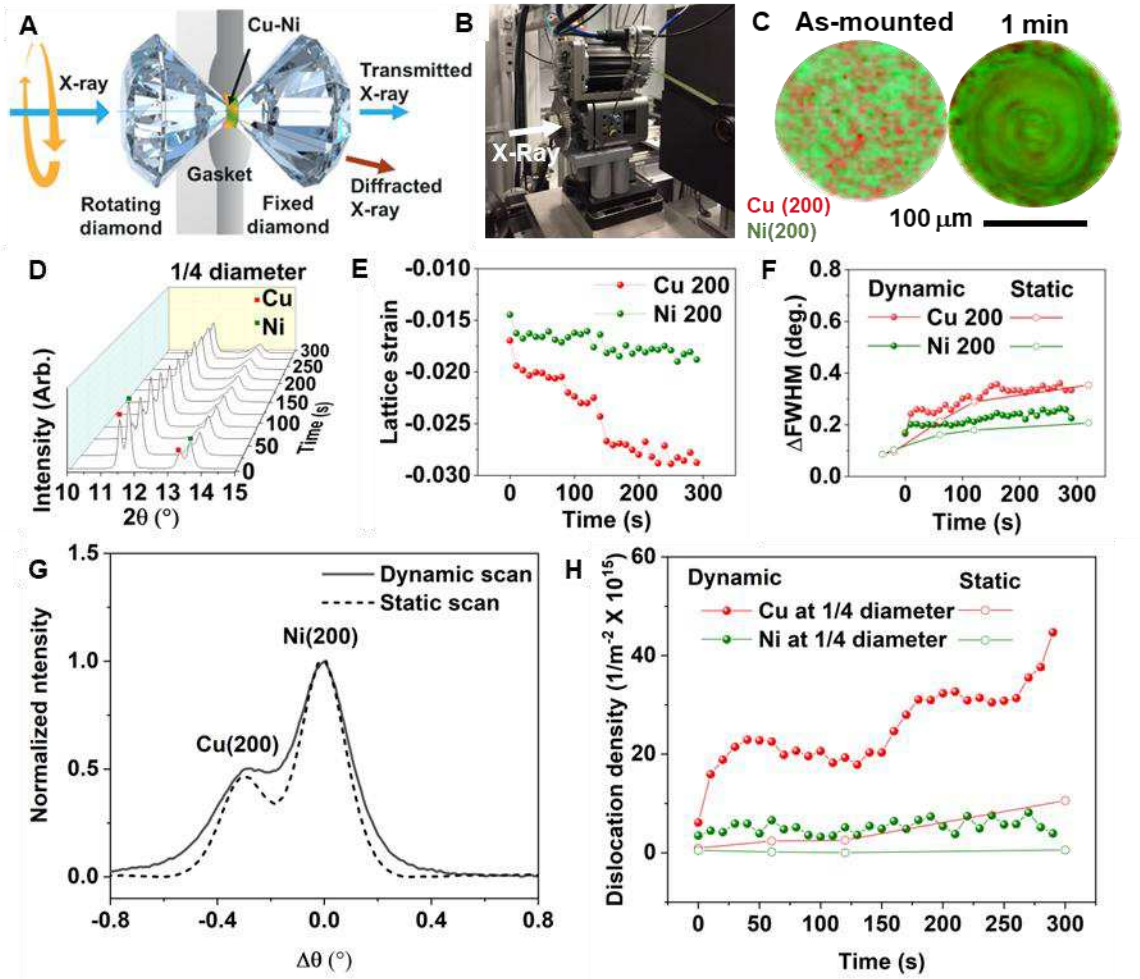


Figure 1: A) HSRDAC schematic. B) Photograph of the HSRDAC assembled at the synchrotron beamline. Static X-ray diffraction imaging of C) as-mounted Cu-Ni powder mixture and after 1 min shear at 10 RPM. D) Time resolved in situ synchrotron XRD at 1/4th diameter. E) Time resolved lattice strain evolution of Cu and Ni during shear. F) Dynamic change of the FWHM of Cu and Ni (200) peaks during shear compared with static measurements of the sheared samples at start and after 1, 2, and 5 min of shear. G) Comparison of X-ray diffraction peaks FWHM during shear (dynamic scan) shown by the black solid line and static scan shown by black dashed line H) Dislocation density changes during shear vs static measurements before and on stopping shear after 1, 2 and 5 min shear.

High resolution, ex situ examination was performed on the final disc (120 μm in diameter/22 μm in thickness) after HSRDAC (10 RPM for 5 min) to understand microstructural evolution as a result of shear deformation at 60 μm radius (schematic in Figure 2A). A scanning electron microscopy energy dispersive spectroscopy (SEM-EDS) map of a full cross section of the disc at 60 μm radius (Figure 2B) revealed substantial intermixing of Cu (red) and Ni (green) within the top 5 μm adjacent to the rotating diamond, and elongated, but largely unmixed, domains of each element persist toward the fixed diamond side.

Bright-field transmission electron microscopy (TEM) imaging of the top 3 μm region near the rotating diamond (Figure 2C) shows extensive nanocrystallization in both Cu and Ni layers. Complementary scanning transmission electron microscopy with EDS (STEM-EDS) analyses (Figures 2D,E) indicated that the intermixed region extended up to approximately 500 nm and displayed nanoscale folded layers of Cu and Ni. To gain further insight on the earlier stage of intermixing, we selected a region below the top 2 μm for STEM-EDS line profile analysis (Figure 2F). The corresponding STEM-EDS map (Figure 2G) illustrated the formation of folds, vortexes, and thin filaments of Cu (shown in red) and Ni (shown in green), along with localized oxygen enrichment at the interfaces (shown in blue). Compositional line profiles (Figure 2H) extracted across a large Cu–Ni interface (marked "1" in Figure 2G) and across a thin Ni filament extending into Cu (marked "2" in Figure 2G, shown in Figure 2I) clearly demonstrate that the degree of intermixing is more pronounced in the thin filament region than at the larger interface.

Atom probe tomography (APT) analysis performed on the top 500 nm region adjacent to the rotating diamond further reveals a complex three-dimensional nanolayered structure in which partially mixed Cu and Ni regions fold and bend over one another (Figure 2J). The corresponding oxygen map from APT (Figure 2K) highlights nanoscale oxide particles (indicated by black arrows) that likely result from the shear-induced fragmentation of native oxides present on the surfaces of the original Cu and Ni powder particles. Two-dimensional compositional maps for Cu, Ni, and O (Figures 2L, 2M, and 2N, respectively) emphasize this nanolayered architecture. Each map is normalized to the element's minimum and maximum concentrations (red indicates the highest concentration, blue the lowest). Curved black dashed lines in Figure 2L denote the Cu–Ni interfaces, and thin white dotted lines point to interdiffusion of Cu along nanocrystalline grain boundaries into Ni-enriched regions. Notably, Figure 2M shows evidence of folding and thinning within the lower Ni layer prior to intermixing, while the oxygen map in Figure 2N (outlined with a black dotted line) underscores the presence of oxide particles at some of the Cu–Ni interfaces.

To further assess the influence of layer thinning on compositional intermixing, we plotted two distinct compositional line profiles. The first profile, taken along the thinned Ni layer (marked by a straight black dashed line, L1, in Figure 2M), is presented in Figure 2O and reveals that thinning leads to considerable intermixing with a composition of roughly 70 at.% Ni and 30 at.% Cu. The second profile, recorded perpendicular to the Cu–Ni interface where both layers are relatively thicker (marked by a straight blue dashed line, L2, in Figure 2M), is shown in Figure 2P and confirms that longer-range intermixing also occurs at these interfaces.

Collectively, these multi-scale observations from micrometer-scale folds and vortex patterns to nanometer-scale layer thinning (approaching sub-10 nm) and the formation of <10 nm fragmented oxide particles, demonstrate the profound impact of high-speed shear deformation on the Cu–Ni powder mixture. Within just 5 minutes of shearing at 10 RPM, the extreme deformation induced a hierarchical nanostructure, thereby validating the HSRDAC's capability to capture rapid microstructural evolution across multiple length scales.

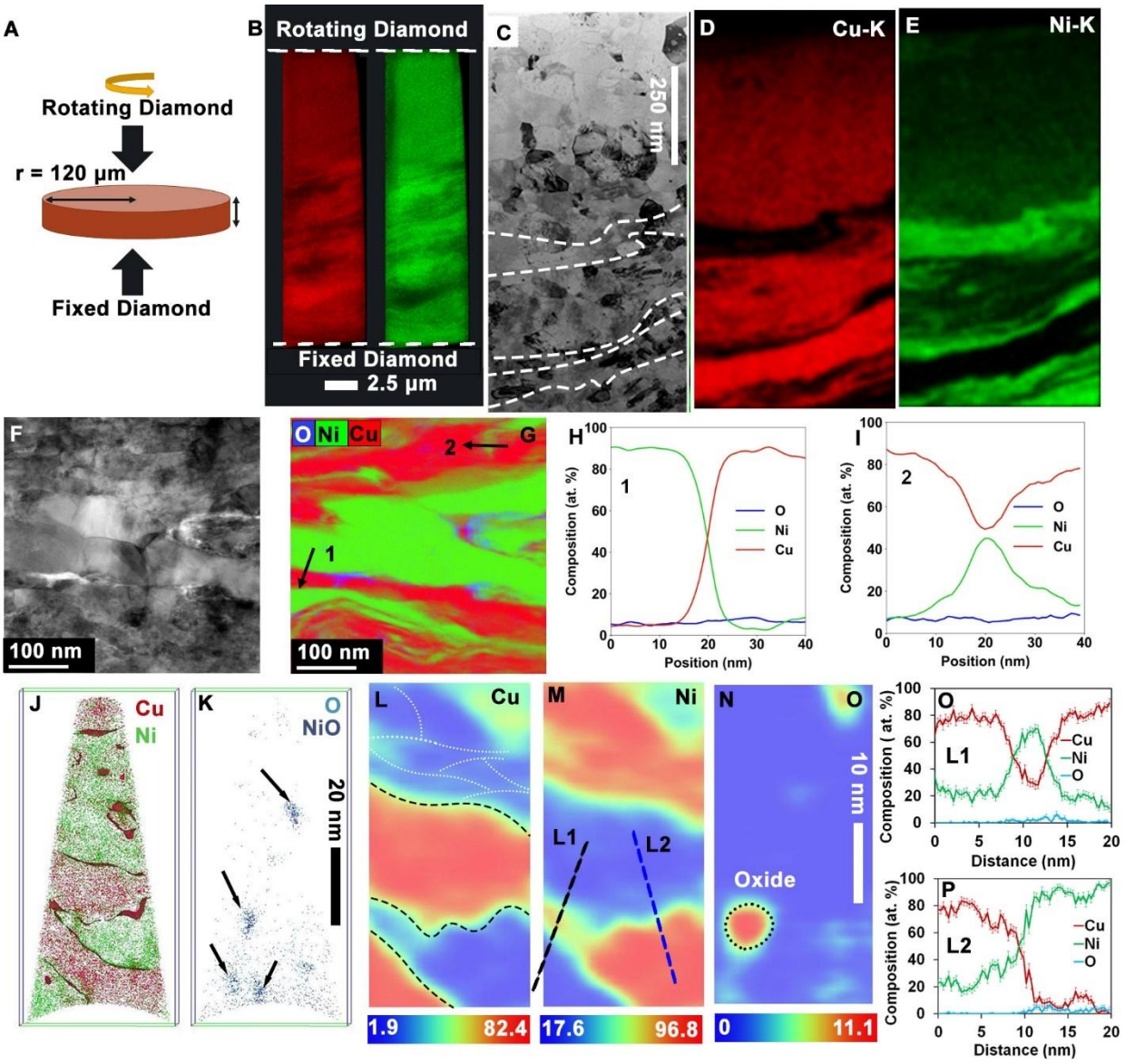


Figure 2: Ex situ multiscale microstructural characterization of shear deformed disk from Cu-Ni powder mixture. A) Schematic of the Cu-Ni disc extracted after HSRDAC shear deformation at 10 RPM for 5 min. B) Through thickness cross sectional SEM EDS maps of Cu (red) and Ni (green) collected from 60 µm from the center of the Cu-Ni disc. The white dashed lines denote the rotating diamond and fixed diamonds. C) TEM image of the top 3 µm of the shear deformed disc revealing nanocrystallization. The Cu-Ni interfaces are marked with white dashed lines. D) STEM-EDS map of the distribution of (D) Cu and (E) Ni in the top 3 µm region adjacent to rotating diamond. (F) STEM image of a sheared Cu-Ni interface region at depth higher than 3 µm from the rotating diamond. (G) Composite STEM EDS map of O, Cu and Ni along with EDS line profiles (H) perpendicular to the Cu-Ni interface marked 1 and (I) across a thin Ni filament marked as 2. (J) APT reconstruction of a region within the top 500 nm thickness of Cu-Ni disc with the interfaces of Cu and Ni marked with a Cu isocomposition surface. (K) Distribution of oxygen and NiO ions within the reconstruction where Oxide regions are marked with black

arrows. 2D compositional maps of Cu-Ni interfaces highlighting the change in (L) Cu (M) Ni and (N) O. The Cu-Ni interfaces are marked with black dashed lines in (L). Cu diffusion to Ni grain boundaries is highlighted with while dotted lines in (L). Two locations chosen for 1D compositional line profiles highlighted as L1 and L2 are given as insets in (M). The 1D composition profiles extracted from L1 and L2 given in (O) and (P) respectively.

To gain insight into the morphological evolution of the Cu–Ni system during shear deformation in the HSRDAC, we performed mesoscale finite element modeling (FEM) simulations. This approach adapts work by M. Pouryazdan et al., which modeled shear-induced mixing in metallic multilayers during high-pressure torsion by treating the materials as incompressible, nonlinear viscous fluids with distinct effective viscosities[22]. In our simulation, we considered a representative domain (44 μm × 22 μm) with a 50% volume fraction of circular Ni particles (with radii ranging from 5 to 10 μm) randomly dispersed within a Cu matrix (Figure 3A). The Cu matrix (red phase) was assigned a reference viscosity of 10^5 Pa·s, while the Ni particles (green phase) were given a higher viscosity defined by a viscosity contrast (VC). Simple shear boundary conditions were applied to the top surface of the domain, using a strain rate of 2.856 s^{-1} and a total strain of 856.80, values estimated from our HSRDAC experiments (see Supplementary equations 2–3). The bottom surface was fixed with a no-slip condition, and periodic boundary conditions were imposed on the lateral boundaries to accommodate the ultrahigh shear strain (Figure 3A).

The FE simulations, conducted with VC of 10, predict the progressive formation of nanolayers as well as folds and vortices (Figures 3B–3E) that agree remarkably well with the structural inhomogeneities and 3D compositional maps observed in our experimental results (Figure 2). Initially, when the strain is small (e.g., at a strain of 11.3), the high-viscosity Ni particles become distinctly elongated (Figures 3B–3C). As the strain increases, these elongated regions are compressed into multiple layers that then start to fold and roll, forming vortex-like structures (Figure 3D). A magnified view (Figure 3E) further reveals striking similarities with the experimental morphologies observed in Figure 2. At high strains, the simulation ultimately shows complete mixing of the two phases (Supplementary Figure 4), reinforcing our experimental observations of dynamic shear-induced microstructural evolution.

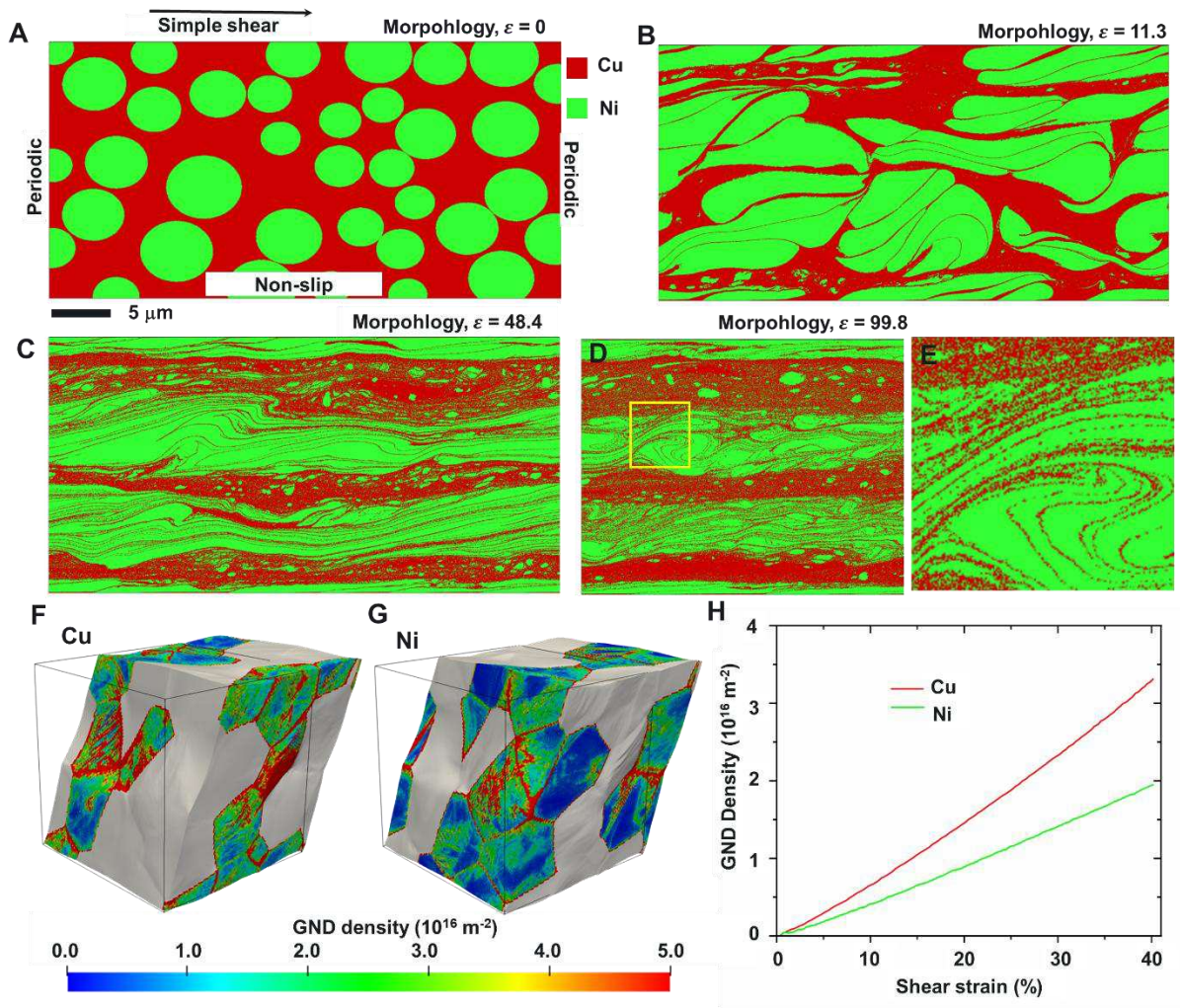


Figure 3: (A) Initial configuration used for finite element simulation of morphological evolution of Cu-Ni. FEM predicted sheared deformed morphology at shear strain ε of (B) 11.3, (C) 48.3 and (D) 99.8. (E) Provides a zoomed in view of the nanolayers showing folds and vortexes that agree well with the morphology revealed by TEM and APT. Crystal plasticity simulations of geometrically necessary dislocations (GND) density at 40% shear strain with the shear strain rate of 2.86/s in (F) Cu and (G) Ni grains. (H) The volume average of GND density in Cu-grains (red), Ni-grains (blue), as a function of % shear strain.

In situ X-ray diffraction during RDAC shear revealed that the dislocation density in Cu evolves more rapidly than in Ni (Figure 1I). To investigate this behavior, we conducted crystal plasticity simulations to examine the accumulation of geometrically necessary dislocations (GNDs) in the early stages of shear deformation. In these simulations, a representative volume element containing equiaxed Cu and Ni grains with an average size of 2 μm was subjected to shear. The results, shown in Figures 3F and 3G, indicate that GND density is higher in Cu than in Ni, which directly correlates with our experimental findings of a higher dislocation density in Cu under dynamic shear conditions.

Building on the experimental observation of nanocrystallization, in which the grains of Cu and Ni are refined from the micron scale to tens of nanometers as evidenced by the ex situ TEM image in Figure 2C, and the nanolayer formation predicted by the FEM simulations (Figures 3B–3E), we sought to investigate the atomic-scale mechanisms underpinning shear-induced dynamic defect evolution and intermixing in the two-phase nanocrystalline Cu–Ni system. To do so, we employed Molecular Dynamics (MD) simulations.

Our initial MD model (Figure 4A) represents a Cu–Ni nanostructure with an average grain size of 17 nm, where Cu atoms are shown in red and Ni atoms in green. At an applied shear strain of 2, the simulated structure becomes noticeably deformed (Figure 4B). Following deformation, we annealed the sample at 300 K; the resulting structure is shown in Figure 4C. In this annealed configuration, atoms arranged in a local hexagonal close-packed (HCP) structure are colored gray, marking stacking faults produced by partial dislocation slip, while blue-colored atoms (those not fitting within either FCC or HCP local structures) highlight regions associated with dislocation cores, defect clusters, and grain boundaries.

Figure 4D presents the evolution of the total dislocation density in Cu (red curve) and Ni (green curve) as a function of applied shear strain. The results confirm that dislocation density increases with strain in both materials, with Shockley partial dislocations dominating due to the small grain sizes[23]. Importantly, Cu exhibits a higher dislocation density than Ni, in agreement with our crystal plasticity simulations and in situ synchrotron XRD data. Upon annealing, a sharp reduction in dislocation density is observed, indicative of recovery processes such as the annihilation of partial dislocations and detwinning, mirroring the experimental observation of lower dislocation densities in static scans after shear compared to dynamic conditions during shear.

In addition to dislocations, MD simulations reveal that shear deformation generates point defects. We tracked the evolution of these defects by defining defect tracers as atoms with a coordination number less than 12, which include atoms in FCC or disordered configurations. As shown in Figure 4E, the kinetics of defect tracer density closely mirror changes in dislocation density, with Ni exhibiting lower defect density than Cu. During annealing, approximately 8% of defect tracers in Cu and 5.6% in Ni recover.

Furthermore, Figure 4F plots the equilibrium vacancy concentrations versus temperature for both Cu and Ni, utilizing their vacancy formation energies (1.27 eV for Cu and 1.57 eV for Ni). The vacancy concentrations estimated from our simulations at an applied strain of 2 correspond to those expected at approximately 1690 K for Cu and 1985 K for Ni, indicating that shear deformation induces defect levels akin to those found at temperatures well above the melting points of the starting metals.

Finally, our MD simulations suggest that grain boundary sliding can play a significant role in the formation of thin interfacial regions between Cu and Ni. Figure 4G illustrates a 2D snapshot of the Cu–Ni interface, where a thin region generated by grain boundary sliding (labeled L2) shows markedly enhanced intermixing compared to a flat interface (labeled L1) (Figure 4 H and I). This atomic-scale intermixing in the thin bands is strikingly similar to the thin strands of Cu and Ni observed in the atom probe tomography (APT) results (Figure 2M).

Collectively, these MD simulations offer an atomic-scale perspective that complements our mesoscale FEM simulations and experimental findings, deepening our understanding of the multiscale, shear-induced microstructural evolution observed in the Cu–Ni system.

In addition, density functional theory (DFT) simulations confirmed that excess vacancies near the Cu–Ni interfaces within thin filaments significantly reduce both the energy barrier and the critical shear strain necessary for further plastic deformation. This reduction in energy cost facilitates enhanced interdiffusion between Cu and Ni, promoting alloying (see Supplementary Section 5).

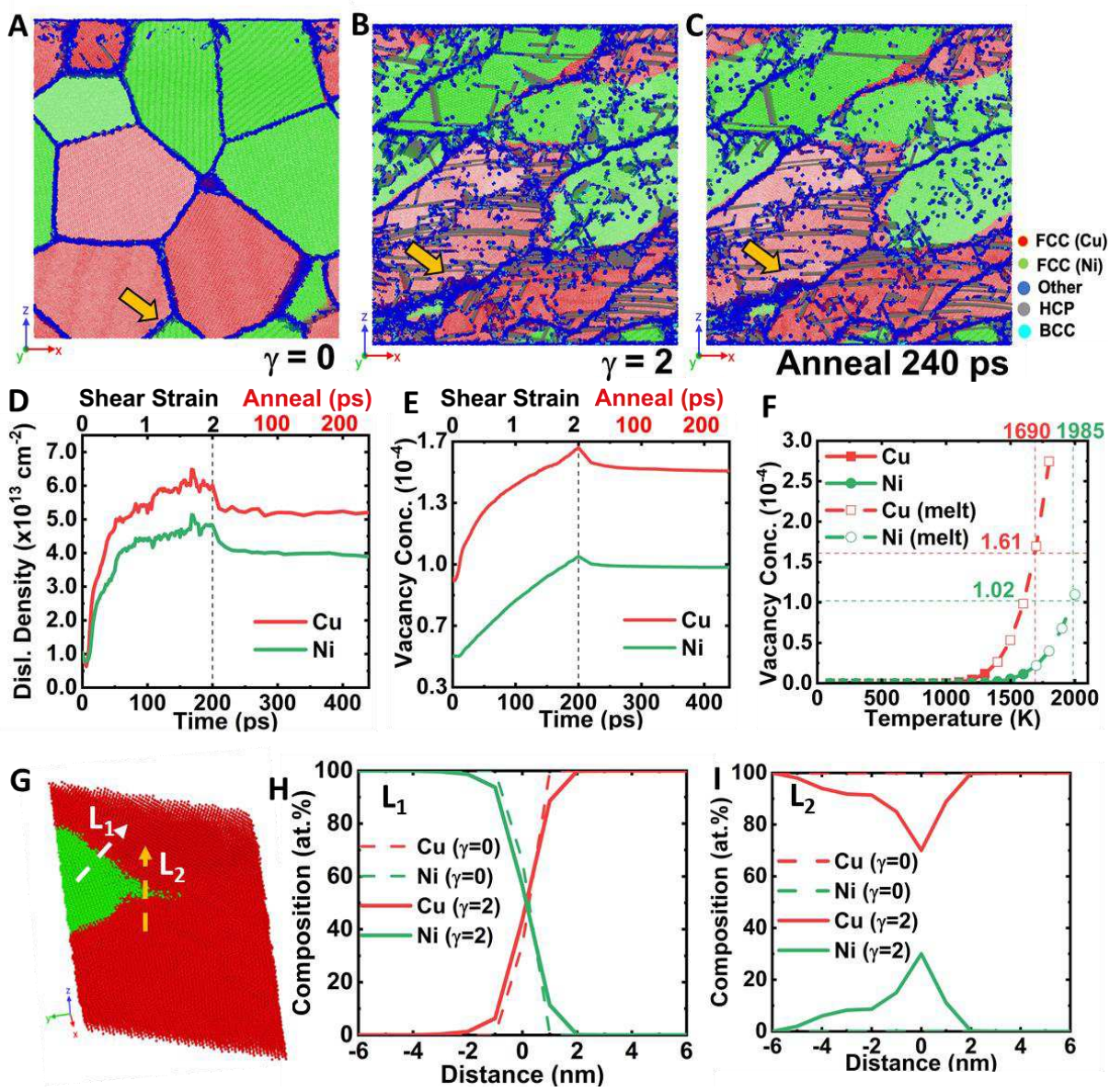


Figure 4: Grain boundary evolution and defect accumulation in Cu/Ni structures under continuous shear deformation by MD. (A) at shear strain 0. (B) shear deformed cell at strain 2. (C) Structure after annealing. (D) Change in total dislocation density in Cu and Ni. (E) Change in vacancy concentration in Cu and Ni. (F) Vacancy concentration as a function of temperature with dashed lines indicating the equivalent temperature for maximum vacancy concentration observed at 2

shear. (G) 2D slice of a region with Cu-Ni interface and a thin region of Ni created by grain boundary sliding. White dashed line in G, denotes the location of a composition profile plotted perpendicular to the interface between the large domains of Cu and Ni (L_1). The composition profile at L_1 is given in (H). The yellow line (L_2) in (G) across the thin Ni region created by grain boundary sliding was used to plot the compositional profile given in I.

Conclusions

In summary, our work establishes a transformative approach for elucidating the dynamic microstructural evolution of materials under extreme shear. Using a novel, high-speed rotational diamond anvil cell (HSRDAC) in conjunction with in situ synchrotron X-ray diffraction, we captured real-time differences in lattice strain and dislocation dynamics between Cu and Ni. Our experiments revealed that Cu exhibits higher lattice strain and dislocation density than Ni during shear loading, with rapid recovery following the cessation of deformation. Complementary ex situ characterization by TEM and APT further revealed the formation of a hierarchical microstructure featuring nanocrystallization, layered morphologies, folds, vortices, and dispersed oxide particles, with layer thinning emerging as a precursor to intermixing.

Multiscale computational simulations provide strong corroboration of these findings. FEM captured the evolution of folds, vortices, and thin layers under ultrahigh shear strain, while crystal plasticity and molecular dynamics simulations revealed that the accumulation of dislocations and point defects is more pronounced in Cu. Moreover, MD illuminated the formation of thin interfacial regions via grain boundary sliding, where DFT further confirmed that excess vacancies lower the energy barrier for plastic deformation and interdiffusion. Together, these complementary approaches reveal a spatially heterogeneous, multi-length- and time-scale dynamic evolution of the Cu–Ni system under shear.

By integrating in situ experimental techniques with advanced ex situ microscopy and multiscale simulations, our study not only fills critical knowledge gaps but also paves the way for the development of novel, energy-efficient solid-phase processing methods. This comprehensive methodology has broad implications for materials engineering, enhanced tribological performance, and even understanding geologic shear processes, representing a significant advancement in the field and offering a powerful tool for future scientific discoveries.

Acknowledgements

This research was supported by the Solid Phase Process Science Initiative, under the Laboratory Directed Research and Development Program at Pacific Northwest National Laboratory (PNNL). A portion of this research was performed using facilities at the Environmental Molecular Sciences Laboratory, a national scientific user facility sponsored by the U.S. Department of Energy (DOE) Office of Biological and Environmental Research and located at PNNL. PNNL is a multi-program national laboratory operated for the DOE by Battelle Memorial Institute under Contract No. DE-AC05-76RL01830. Portions of this This research was performed on APS beam time award(s) (DOI: https://doi.org/10.46936/APS-180008/60009532) from the Advanced Photon Source, a U.S. Department of Energy (DOE) Office of Science user facility operated for the DOE Office of Science by Argonne National Laboratory under Contract

No. DE-AC02-06CH11357. HPCAT operations are supported by DOE-NNSAs Office of Experimental Sciences. The ab initio calculations were performed using PNNL Institutional Computing (PIC) service.

Author contributions

Conceptualization, Funding acquisition, project administration, supervision: AD. Methodology, investigation, visualization: TL, CP, SS, MO, BG, LL, NC, WF, SMu, SMa, YL, AS, SH, PS, CP, AD. Writing of original draft, review and editing: AD with input from all authors.

References

1 Bridgman, P. W. in *Volume V Collected Experimental Papers, Volume V* 3001-3017 (Harvard University Press, 1964).

2 Dowding, I. & Schuh, C. A. Metals strengthen with increasing temperature at extreme strain rates. *Nature* **630**, 91-95 (2024). https://doi.org/10.1038/s41586-024-07420-1

3 Edalati, K. *et al.* Severe plastic deformation for producing superfunctional ultrafine-grained and heterostructured materials: An interdisciplinary review. *Journal of Alloys and Compounds* **1002**, 174667 (2024). https://doi.org/https://doi.org/10.1016/j.jallcom.2024.174667

4 Greiner, C., Gagel, J. & Gumbsch, P. Solids Under Extreme Shear: Friction-Mediated Subsurface Structural Transformations. *Advanced Materials* **31**, 1806705 (2019). https://doi.org/https://doi.org/10.1002/adma.201806705

5 Edalati, K. *et al.* Nanomaterials by severe plastic deformation: review of historical developments and recent advances. *Materials Research Letters* **10**, 163-256 (2022). https://doi.org/10.1080/21663831.2022.2029779

6 Kerber, M. B. *et al.* In Situ Synchrotron X-Ray Diffraction during High-Pressure Torsion Deformation of Ni and NiTi. *Advanced Engineering Materials* **23**, 2100159 (2021). https://doi.org/https://doi.org/10.1002/adem.202100159

7 Valiev, R. Z., Islamgaliev, R. K. & Alexandrov, I. V. Bulk nanostructured materials from severe plastic deformation. *Progress in Materials Science* **45**, 103-189 (2000). https://doi.org/https://doi.org/10.1016/S0079-6425(99)00007-9

8 Sirorattanakul, K., Larochelle, S., Rubino, V., Lapusta, N. & Rosakis, A. J. Sliding and healing of frictional interfaces that appear stationary. *Nature* **639**, 947-953 (2025). https://doi.org/10.1038/s41586-025-08673-0

9 Bellon, P., Averback, R. S., Ren, F., Pant, N. & Ashkenazy, Y. A Review: Microstructural and Phase Evolution in Alloys during Extended Plastic Deformation. *JOM* **73**, 2212-2224 (2021). https://doi.org/10.1007/s11837-021-04709-8

10 Samae, V. *et al.* Stress-induced amorphization triggers deformation in the lithospheric mantle. *Nature* **591**, 82-86 (2021). https://doi.org/10.1038/s41586-021-03238-3

11 Han, Y. *et al.* Recent progress in the application of rotational diamond anvil cell. *APL Materials* **11** (2023). https://doi.org/10.1063/5.0156748

12 Vauchez, A., Tommasi, A. & Mainprice, D. Faults (shear zones) in the Earth's mantle. *Tectonophysics* **558-559**, 1-27 (2012). https://doi.org/https://doi.org/10.1016/j.tecto.2012.06.006

13 Levitas, V. I. High-Pressure Phase Transformations under Severe Plastic Deformation by Torsion in Rotational Anvils. *MATERIALS TRANSACTIONS* **60**, 1294-1301 (2019). https://doi.org/10.2320/matertrans.MF201923

14 Levitas, V. I. High-pressure mechanochemistry: Conceptual multiscale theory and interpretation of experiments. *Phys Rev B* **70** (2004). https://doi.org/ARTN 184118

10.1103/PhysRevB.70.184118
15 Levitas, V. I. & Shvedov, L. K. Low-pressure phase transformation from rhombohedral to cubic BN: Experiment and theory. *Phys Rev B* **65** (2002). https://doi.org/ARTN 104109

10.1103/PhysRevB.65.104109
16 Ma, Y. Z., Levitas, V. I. & Hashemi, J. X-ray diffraction measurements in a rotational diamond anvil cell. *J Phys Chem Solids* **67**, 2083-2090 (2006). https://doi.org/10.1016/j.jpcs.2006.05.052
17 Ji, C. *et al.* Shear-induced phase transition of nanocrystalline hexagonal boron nitride to wurtzitic structure at room temperature and lower pressure. *P Natl Acad Sci USA* **109**, 19108-19112 (2012). https://doi.org/10.1073/pnas.1214976109
18 McCulloch, D. G. *et al.* Investigation of Room Temperature Formation of the Ultra-Hard Nanocarbons Diamond and Lonsdaleite. *Small* **16** (2020). https://doi.org/ARTN 2004695

10.1002/smll.202004695
19 Huston, L. Q. *et al.* Synthesis of Novel Phases in Si Nanowires Using Diamond Anvil Cells at High Pressures and Temperatures. *Nano Lett* **21**, 1427-1433 (2021). https://doi.org/10.1021/acs.nanolett.0c04354
20 Overman, N. R. *et al.* Microstructural progression of shear-induced mixing in a CuNi alloy. *Materials Characterization* **171**, 110759 (2021). https://doi.org/https://doi.org/10.1016/j.matchar.2020.110759
21 Kilmametov, A. R. *et al.* Microstructure evolution in copper under severe plastic deformation detected by in situ X-ray diffraction using monochromatic synchrotron light. *Materials Science and Engineering: A* **503**, 10-13 (2009). https://doi.org/https://doi.org/10.1016/j.msea.2008.11.023
22 Pouryazdan, M., Kaus, B. J. P., Rack, A., Ershov, A. & Hahn, H. Mixing instabilities during shearing of metals. *Nature Communications* **8**, 1611 (2017). https://doi.org/10.1038/s41467-017-01879-5
23 Zhu, Y. T., Liao, X. Z. & Wu, X. L. in *Progress in Materials Science* Vol. 57 1-62 (Pergamon, 2012).

Supplementary Files

This is a list of supplementary files associated with this preprint. Click to download.

- Supplementaryinformation2Feb26.docx